

Experimental validation of digital periodic error correction

Tony L. Schmitz¹, Lonnie Houck III¹, David Chu², and Lee Kalem²

¹University of Florida, Dept. of Mechanical and Aerospace Engineering, Gainesville, FL

²Agilent Technologies, Inc., Santa Clara, CA

1.0 Introduction

Differential-path interferometry is used extensively in situations requiring accurate displacement measurements. In many applications, a dual frequency (heterodyne) Michelson-type interferometer with single, double, or multiple passes of the optical paths is implemented. These systems infer changes in displacement of a selected optical path by monitoring the optically-induced variation in a photodetector current. The phase-measuring electronics convert this photodetector current to displacement by digitizing the phase progression of the photodetector signal. Due to non-ideal performance, mixing between the two heterodyne frequencies may occur, which results in periodic errors superimposed on the desired displacement data [1-5]. In practice, first-order periodic error, which appears as single sideband modulation on the data at a spatial frequency of one cycle per displacement fringe, often dominates. Second-order periodic error, with a spatial frequency of two cycles per displacement fringe, is also commonly observed.

Although modifications to traditional optical setups may be implemented to reduce periodic error, it is often inconvenient to make changes to existing optical setups. Additionally, the extra optical components and/or hardware generally necessary to achieve decreased periodic error can be costly. As an alternative to changes in the interferometer setup, Chu and Ray have recently described a scheme to correct first-order periodic error in real-time using digital logic hardware [6].

The purpose of this study is to validate the Chu and Ray approach using a bench-top setup of a single-pass, heterodyne Michelson-type interferometer. The setup enables: 1) isolation of periodic error as the primary uncertainty source in displacement measuring interferometry; and 2) variation of the frequency mixing that leads to periodic error so that the error amplitude may be changed. During target motion, the real-time first-order error correction is digitally applied in hardware and both the corrected and uncorrected measurement signals are recorded.

2.0 Setup description

A photograph of the setup is provided in Fig. 1. The orthogonal, linearly polarized beams with a split frequency of approximately 3.65 MHz generated within the Helium-Neon laser first pass through a half wave plate. Rotation of the half wave plate enables variation in the apparent angular alignment (about the beam axis) between the polarization axes and polarizing beam splitter; deviations in this alignment lead to frequency mixing in the interferometer. The light is then incident on a non-polarizing beam splitter (80% transmission) that directs a portion of the beam to a fiber optic pickup after passing through a fixed angle sheet polarizer (oriented at nominally 45 deg to the laser orthogonal polarizations). The pickup is mounted on a two degree-of-freedom flexure which enables efficient coupling of the light into the multi-mode fiber optic. This signal is used as the phase reference in the measurement electronics.

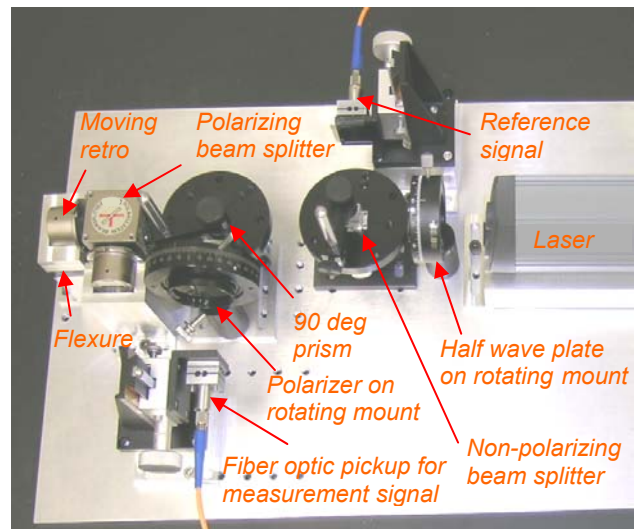


Figure 1: Photograph of bench-top setup for single-pass heterodyne interferometer.

The remainder of the light continues to the polarizing beam splitter where it is nominally separated into its two frequency components that travel separately to the moving and fixed retroreflectors. In this design, motion of the moving retroreflector is achieved using a parallelogram, leaf-type flexure. This enables nominally linear, oscillating displacement at a

single frequency. The harmonic motion profile: 1) includes constantly varying velocity, acceleration, and jerk levels that are conveniently adjusted by varying the displacement amplitude; and 2) provides a rigorous test of the digital periodic error correction algorithm which assumes negligible jerk. After the beams are recombined in the polarizing beam splitter, they are directed by a 90 deg prism through a polarizer. Rotation of the polarizer changes the relative amplitude of the intended and mixing-induced interference signals and, therefore, the periodic error. Finally, the light is launched into a fiber optic pickup. This serves as the measurement signal in the measurement electronics.

As noted, the intent of the setup design was to minimize other well-known error contributors and enable variation in the periodic error nature (i.e., first- or second-order) and amplitude. To isolate periodic error, the setup was designed with zero Abbe offset (i.e., the measurement axis was collinear with the motion axis) and zero dead path difference (i.e., the distance between the polarization beam splitter and the moving retroreflector was equal to the distance between the polarization beam splitter and the fixed retroreflector at initialization). The measurement time (100 ms) and motion amplitude (<200 μm) were kept small to minimize the contribution of air refractive index variations due to the environmental changes. Additionally, the flexure small motion amplitude leads to small beam shear (using the flexure dimensions and material properties, the maximum parasitic displacement perpendicular to the beam axis was calculated to be 0.1 nm for a 100 μm motion amplitude) and angular error (3×10^{-3} μrad for a 100 μm motion amplitude) [7].

Error contributors which were not well-controlled by this setup include cosine error, or an angular misalignment between the measurement and motion axes, due to the small displacement range and mechanical noise (the flexure's low stiffness and light damping caused table vibrations to be transmitted to the moving retroreflector, although these were reduced somewhat by mounting the entire assembly on a rubber mat). However, this study is unique in that the error correction was applied digitally. The analog measurement signal was sampled (0.3 nm resolution) and then the first-order periodic error correction was applied to the digitized data. Because our intent was to

compare the (digitized) corrected and uncorrected signals, the cosine and mechanical noise errors can be considered common mode and have little impact on the final results presented here.

3.0 Experimental results

In this section, we describe the analysis procedure used to extract periodic error from the moving retroreflector displacement and present results for various angular orientations of the half wave plate and polarizer. Data was collected by first initiating flexure motion using a light impact (applied by a rubber-tipped mallet) and then recording displacement at 312.5 kHz during the resulting harmonic motion.

3.1 Data analysis method

For a unidirectional, constant velocity motion, periodic error can be identified in an interferometer signal by subtracting the least squares straight line fit from the data. In this case, the gross flexure motion is best represented by an exponentially decaying sine wave with some initial phase and, potentially, a DC offset depending on the initially displacement value of the interferometer. To remove the gross motion and isolate the periodic error, a nonlinear least squares fit to the data was performed using a function of the form $x(t) = \delta + Ae^{-\zeta\omega_n t} \sin(\omega_d t + \alpha)$, where δ is the DC offset, A is the amplitude, ζ is the viscous damping ratio, ω_n is the undamped natural frequency, $\omega_d = \omega_n \sqrt{1 - \zeta^2}$ is the damped natural frequency, and α is the initial phase. Once the fit parameters were determined, this function was subtracted from the uncorrected and corrected (first-order error removed) signals and the periodic error levels compared. Typical values for ω_n and ζ were 248.6 rad/s (39.6 Hz) and 0.009 (0.9% damping), respectively.

Example results for the fitting procedure are provided in Fig. 2. A portion of the gross uncorrected motion (solid line) and nonlinear least squares fit (dotted line) are shown in panel a). These signals are then differenced to isolate the periodic error. Panel b) shows the result for a high velocity section of the original signal, while panel c) shows the result for a low velocity portion. In both cases, the dominant first-order error created by angular misalignment of the polarizer is effectively removed by the correction algorithm. It may also be noted that the least squares fit does not exactly capture the actual

motion due to the small curvature and DC offset observed in both panels b) and c); however, the low spatial frequency and DC offset errors do not significantly affect the subsequent frequency domain analysis of the periodic error amplitudes before and after correction.

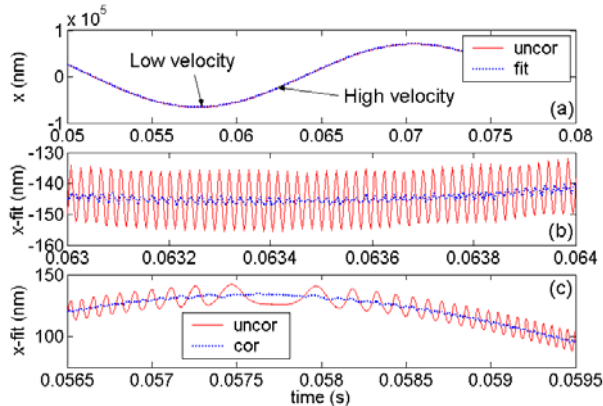


Figure 2: Example results from data analysis: a) uncorrected gross flexure motion with sinusoidal nonlinear least squares fit superimposed; b) difference between motion and fit in high velocity region; and c) difference in low velocity region.

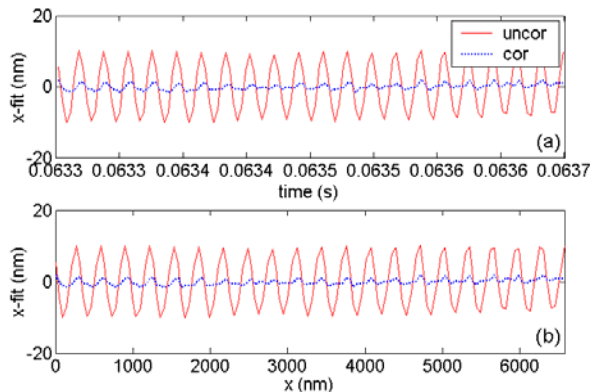


Figure 3: First-order periodic error reduction example: a) error vs. time for uncorrected (solid line) and corrected (dotted line) signals; b) error vs. uncorrected displacement.

A subset of the high velocity data shown in Fig. 2b) is reproduced in Fig. 3a) (the DC offset has been removed) and replotted versus uncorrected position in 3b). For the single pass Helium-Neon interferometer setup used here, first-order error repeats every $633/2 = 316.5$ nm, while second-order completes a full cycle in $633/4 = 158.3$ nm. It is now clearly observed that the signal is dominated by first-order error in this case. To identify the first- and second-order error amplitudes, the Fast Fourier transform of the error (vs. displacement) was computed and the spatial frequency axis normalized to periodic

error order; see Fig. 4. It is shown that the first-order error magnitude has been reduced from 8.4 nm to 0.9 nm.

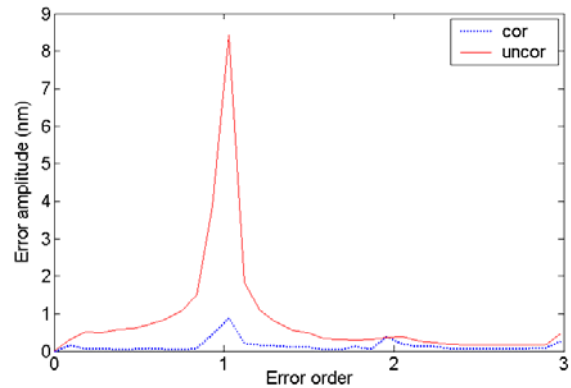


Figure 4: Fast Fourier transform of error vs. displacement data for corrected (dotted line) and uncorrected (solid line) signals. The first-order error is reduced from 8.4 nm to 0.9 nm.

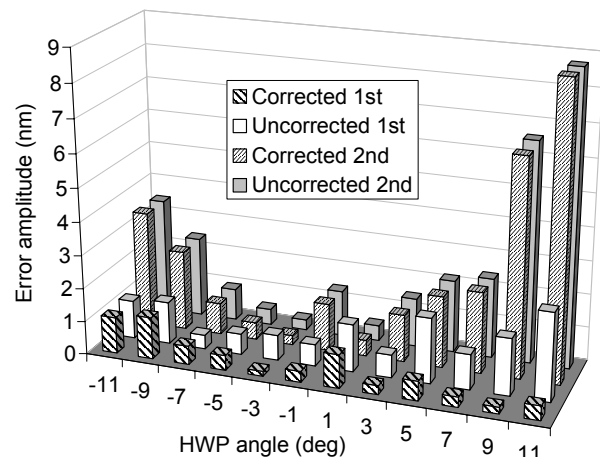


Figure 5: Variation in first- and second-order periodic error with changes in half wave plate orientation. Results for both the uncorrected and corrected signals are provided.

3.2 Error variation with interferometer setup

To explore the independent influences of the half wave plate and polarizer orientations, tests were carried out where one orientation was fixed and the other varied about a nominal value. To represent the results, the uncorrected and corrected first- and second-order periodic error amplitudes were extracted for each orientation. Figure 5 shows the results for a fixed (nominally 45 deg) polarizer angle and an ± 11 deg variation in the half wave plate angle. While the trend in both error orders is increased amplitude with larger departure from the nominal orientation, the second-order error is more strongly affected.

Figure 6 displays the results for a variable polarizer angle with a fixed half wave plate angle (the fast axis was nominally aligned with one of the linear polarization directions). In this case, the first-order error is more strongly influenced. In all instances, the correction scheme reduces the first-order periodic error to sub-nm levels. As before, the second-order amplitudes are not affected.

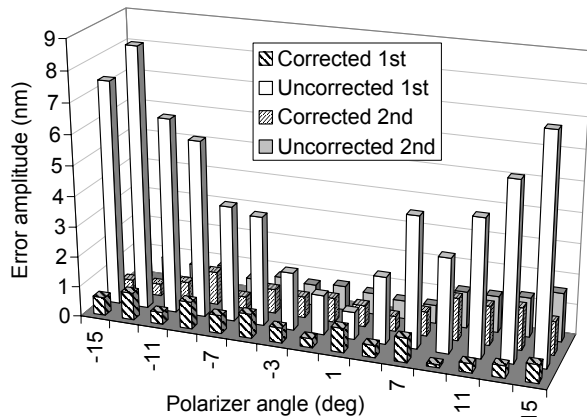


Figure 6: Variation in first- and second-order periodic error with changes in polarizer orientation. Results for both the uncorrected and corrected signals are provided.

3.3 Repeatability

The final measurement activity was to evaluate the repeatability of the periodic error amplitudes. To complete this task, displacement was recorded for 15 separate impacts of the flexure-mounted moving retroreflector. Half wave plate and polarizer angles were selected to minimize periodic error. The analysis described in Section 3.1 was then completed for each data record and the first- and second-order periodic error amplitudes determined for both the uncorrected and corrected cases. The results are shown in Fig. 7. The standard deviations for the error amplitudes were less than 0.2 nm (first-order) and 0.3 nm (second-order) for the 15 data sets. This compares favorably with the 0.3 nm displacement resolution for the interferometer used in this study.

4.0 Conclusions

Experimental validation of the digital first-order periodic error reduction scheme described by Chu and Ray [6] was completed using a bench-top setup of a single-pass, heterodyne Michelson interferometer. The strategy was to minimize common error contributors such as Abbe, dead path, and environmental errors

through the setup design in order to isolate periodic error. Linear, oscillating motion generation was accomplished using a parallelogram, leaf-type flexure. The setup also enabled variation of the periodic error through independent rotation of a half wave plate and polarizer. Experimental results demonstrated that the correction algorithm can successfully attenuate first-order error to sub-nm levels for a wide range of frequency mixing conditions.

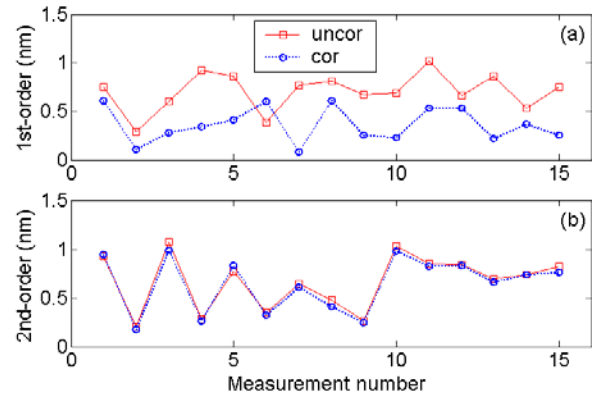


Figure 7: Repeatability testing results for nominal orientations of half wave plate and polarizer: a) first-order error amplitudes; and b) second-order error amplitudes.

5.0 Acknowledgements

This work was funded by a grant from Agilent Technologies, Inc.

6.0 References

1. Fedotova G. Analysis of the measurement error of the parameters of mechanical vibrations. *Measurement Techniques* 1980; 23(7):577-580.
2. Quenelle R. Nonlinearity in interferometric measurements. *Hewlett-Packard Journal* 1983; 34(4):10.
3. Sutton C. Nonlinearity in length measurements using heterodyne laser Michelson interferometry. *Journal of Physics E: Scientific Instrumentation* 1987; 20:1290-1292.
4. Barash V, Fedotova G. Heterodyne interferometer to measure vibration parameters. *Measurement Techniques* 1984; 27(7):50-51.
5. Bobroff N. Residual errors in laser interferometry from air turbulence and nonlinearity. *Applied Optics* 1987; 26(13):2676-2682.
6. Chu D, Ray A. Nonlinearity measurement and correction of metrology data from an interferometer system. In: *Proceedings of 4th euspen International Conference*, Glasgow, Scotland (UK). May-June, 2004. pp. 300-301.
7. Smith ST. *Flexures: Elements of Elastic Mechanisms*. Amsterdam: Gordon and Breach Science Publishers, 2000.